Homogeneous Catalysis in Plastic Waste Upcycling
A DFT Study on the Role of Imperfections in Polymer Chains

Kolganov, Alexander A.; Avadakkam, S.A.; Pidko, Evgeny A.

DOI
10.1021/acscatal.3c03269

Publication date
2023

Document Version
Final published version

Published in
ACS Catalysis

ACS Catalysis

pubs.acs.org/acscatalysis
Research Article

Homogeneous Catalysis in Plastic Waste Upcycling: A DFT Study on the Role of Imperfections in Polymer Chains

Alexander A. Kolganov, A. Sreenithya, and Evgeny A. Pidko*

Cite This: ACS Catal. 2023, 13, 13310−13318
Read Online

ACCESS | Metrics & More | Article Recommendations | Supporting Information

ABSTRACT: Rational plastic recycling is critical for addressing the environmental challenges associated with plastic waste. Among the various recycling methods, chemical recycling, particularly via homogeneous catalysis, holds promise for converting plastic waste into valuable products. Post-consumer polymer wastes could present a challenge for catalytic upcycling due to the structural inhomogeneity and functionalization of the polyolefin chains. The impact of substrate aging on the performance of the upcycling catalyst can be viewed as an "inverse problem" of heterogeneous catalysis and has not received sufficient attention in mechanistic studies on this subject. Herein, we present a density functional theory study on the dehydrogenative upcycling of polyethylene (PE) with different in-chain impurities, representing the chemistry of post-consumption PE wastes. We selected the (^{tBu4}POCOP)-Ir pincer complex catalyzed dehydrogenation of PE as our model reaction. The calculations reveal that common in-chain impurities found in PE, such as carbonyl, hydroxyl, epoxides, and chlorine atoms, inhibit the overall catalyst performance. These impurities form stable molecular complexes with the catalyst, leading to a substantial increase in the energy barriers of the initial reaction step, the C−H bond addition. We also observe that the reaction on the ideal crystalline PE is also impeded. However, highly distorted PE chains exhibit greater susceptibility toward the (^{tBu4}POCOP)-Ir catalyst. Our mechanistic studies demonstrated that the reaction on the side alkane chains is kinetically favorable compared with the reaction on the PE backbone. The study highlights the critical role of in-chain heterogenieties in the catalytic activation of polymer chains and provides valuable insights into the development of effective technologies for upcycling plastic waste.

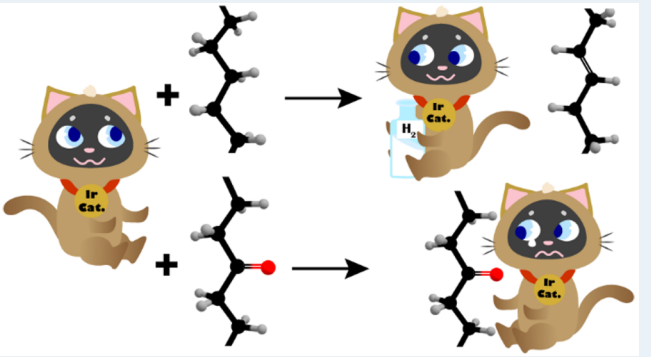

KEYWORDS: *plastic upcycling, homogeneous catalysis, density functional theory, catalytic dehydrogenation*

1. INTRODUCTION

Commercial plastics have experienced extensive utilization across diverse industries due to their affordability, lightweight nature, and versatile properties, making them indispensable for numerous consumer goods and packaging materials. However, the accumulation of plastic waste has emerged as a significant environmental concern, primarily attributable to its persistent nature and prolonged environmental degradation. It is crucial to recognize that, despite the environmental challenges posed by plastics, their inherent characteristics render them essential, thus positioning them as a "necessary evil". Consequently, instead of solely focusing on the eradication of commercial plastics, it becomes imperative to prioritize the development and implementation of effective recycling strategies that mitigate the environmental impacts associated with their accumulation.

Unfortunately, only a small fraction of plastic waste is currently recycled.[1] The conventional mechanical recycling methods often result in degraded properties, limiting the potential for the reuse of recycled plastics in their original applications.[2,3] To address this issue, chemical upcycling has emerged as an attractive solution, which involves converting waste polyolefins into value-added materials and products, thus establishing a basis for the circular economy.[4,5] Several processes have been proposed for the plastics' chemical upcycling, including pyrolysis,[6,7] cracking,[8,9] hydrogenolysis,[10−13] and advanced oxidation.[14,15] Transfer dehydrogenation of polyethylene forms an important and common mechanistic event in many of the recently developed upcycling processes such as isomerizing ethenolysis, dehydroaromatization, and olefin metathesis (Scheme 1(a)).[16−18] Introducing tunable amounts of unsaturation in the polyolefin chains opens the way toward the various plastic waste valorization pathways, e.g. ethenolysis,[18] metathesis,[16,17] and dehydroaromatization.[25] The key step of the dehydrogenation is the activation of the inert C−H bond, which introduces a certain challenge.[26−28]

Received: July 17, 2023
Revised: August 30, 2023
Published: October 2, 2023

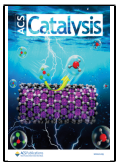

https://doi.org/10.1021/acscatal.3c03269
ACS Catal. 2023, 13, 13310−13318

Scheme 1. a) Ir Pincer Catalyzed Polyethylene (PE) Dehydrogenation Reaction as the Key Step in Different Upcycling Processes Leading to Value Added Products, b) Different Functional Group Impurities (X, Epoxo, and Carbonyl) Present on the PE Chain, and c) Our Hypothesis for the Deactivation of the Ir Pincer Catalyst by the Impurities Present in the PE Chain

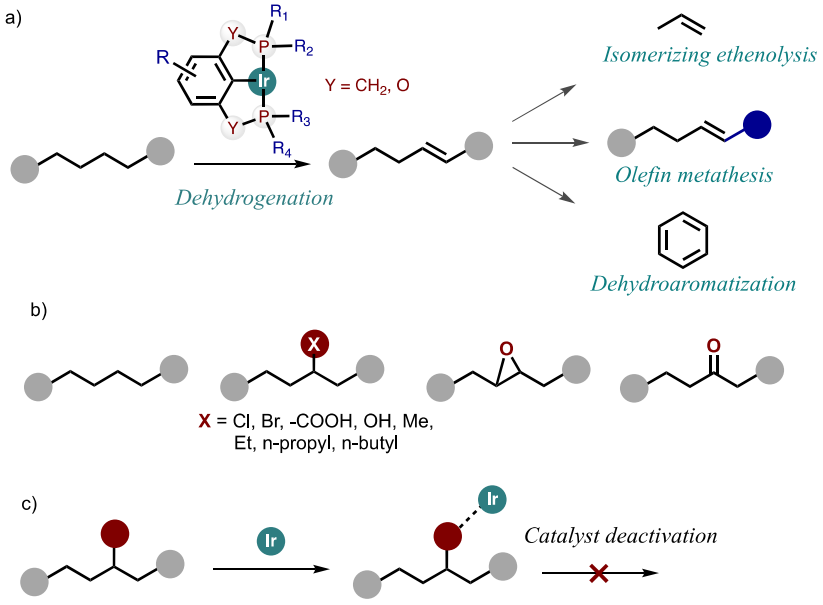

Plastic waste is frequently contaminated with impurities[19,20] and after being exposed to the environment for extended periods in soil or water may also contain impurities resulting from the aging process (Scheme 1(b)).[21] For example, photodegradation of polyethylene under UV light generates free radicals that can cause chain scission, branching, and cross-linking.[22] Additionally, PE aging can lead to the formation of in-chain impurities containing oxygen, such as hydroxyl or carbonyl groups.[21,23] The impact of these impurities is well-documented in the context of catalytic pyrolysis, where the presence of Cl and N in the plastic waste could rapidly deactivate the catalyst.[20,24] However, the effect of these impurities on the processing of polyethylene waste through homogeneous chemical upcycling remains uncertain. We hypothesize (Scheme 1(c)) that the presence of in-chain defects in polyethylene could induce organometallic catalyst deactivation. For instance, the in-chain impurities may bind strongly to the catalytic species and impede further reactions.

Herein, we present a density functional theory study on the dehydrogenative upcycling of polyethylene (PE) with different in-chain impurities, representing the chemistry of post-consumption PE wastes. As a model reaction, we have selected the first step of the PE upcycling proposed by Conk et al.,[18] the (^{tBu4}POCOP)-Ir pincer complex catalyzed homogeneous dehydrogenation of polyethylene. We have carried out the DFT study of the reaction path of dehydrogenation of the (^{tBu4}POCOP)-Ir pincer on the differently modified PE chains. Different catalytic paths promoted by a representative model homogeneous (^{tBu4}POCOP)-Ir pincer catalyst were investigated. We aimed to highlight the factors influencing the intrinsic reactivity of the homogeneous catalysts for plastic waste valorization.

2. COMPUTATIONAL DETAILS

Crystalline polyethylene with two *all-trans* CH_2 chains with DFT-optimized lattice parameters of a = 2.55 Å; b = 4.92 Å; and c = 7.15 Å[29,30] (12 × 12 × 6 k-point mesh) was used as an initial model. Calculations were carried out for the 7 × 7 × 3 supercell to simulate crystalline polyethylene. This model was terminated along the y-axis where 25 Å of vacuum was added to simulate the PE surface. All except one chain were removed from the 7 × 7 × 3 supercell model for the calculation of the isolated PE chains. The resulting unit cell formulas are $C_{210}H_{420}$ and $C_{14}H_{28}$ for the crystalline PE and isolated chains, respectively. The computations employed periodic boundary conditions (PBCs).

All calculations were carried out using the Vienna *Ab Initio* Simulation Package (VASP 5.4.4).[31,32] The exchange-correlational energy term was described by the generalized gradient approximation PBE functional[33] with D3(BJ) dispersion correction.[34,35] The solvent environment (*p*-xylene) was simulated implicitly *via* the VASPsol code.[36,37] A plane wave basis set with a cutoff energy of 450 eV was used in combination with the projected augmented wave (PAW) method.[38] The Brillouin zone sampling was restricted to the Γ point. The geometry convergence was assumed to be reached when all atomic forces were below 0.04 eV Å^{-1}. During the geometry optimization, all atoms were allowed to relax.

The climbed image nudged-elastic band method (CI-NEB) was used to determine the minimum energy path and to guess the transition state structures.[39] The number of images for the CI-NEB method was set as 8 or 16. The maximum energy geometry along the reaction path generated by the CI-NEB method was further optimized by the Quasi-Newton method. The transition states were confirmed by the presence of a single imaginary frequency along the reaction coordinate.

3. RESULTS AND DISCUSSION

3.1. Dehydrogenation of the Pristine PE. We initiated our investigation by examining the reaction on pristine polyethylene without any impurities to establish a benchmark for comparison. The general mechanism of the catalytic polyolefin dehydrogenation by Ir(I) pincer catalyst **C1** is presented in Scheme 2. The catalytic reaction starts with the C−H oxidative addition in catalyst-substrate complex **1** between Ir catalyst **C1** and PE resulting in Ir(III)H(R) intermediate **2** (Scheme 2). Next, a β-H elimination step in **2** yields the

https://doi.org/10.1021/acscatal.3c03269
ACS Catal. 2023, 13, 13310−13318

Scheme 2. Catalytic Cycle for the (^{tBu4}POCOP)-Ir Catalyzed Transfer Dehydrogenation of PE

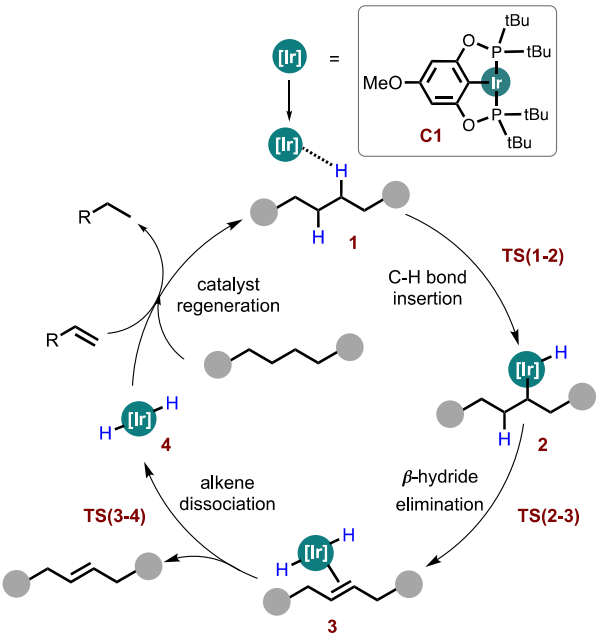

dehydrogenated PE chain π-bound with the (^{tBu4}POCOP)-IrH$_2$ species **3**. In the next step, the alkene dissociates, and the (^{tBu4}POCOP)-IrH$_2$ species **4** is formed. Sacrificial hydrogenation of an alkene with **4** regenerates Ir catalyst **C1**, which then forms complex **1** with PE, and the catalytic cycle continues. In this study, we have computed the energetics associated with the dehydrogenation of PE from starting complex **1** to the alkene dissociation step resulting in intermediate **4**. A parallel catalyst regeneration cycle is present in Scheme S1 of the Supporting Information. We calculated the reaction pathways for both polyethylene crystals and isolated polyethylene chains, aiming to assess the influence of the polyethylene state (crystalline or isolated chain) on the reaction path. The reaction was calculated for the in-chain dehydrogenation, for which high regeoselectivity of (^{tBu4}POCOP)-Ir pincer was experimentally demonstrated.[18,40] For the crystalline PE, we have modeled the reaction on the top central chain of the crystal surface.

For the isolated PE chain, the initial C−H oxidative addition step [**TS(1−2)**] has a barrier of 66 kJ/mol. In the resulting intermediate **2**, the adjacent C−H bonds are *trans* to the C−Ir bond. The PE chain has to undergo a conformational change [**TS(2−2′)**] to enable the β-hydride elimination step facilitated by an agostic Ir···C−H interaction in **2**. While this mechanistic step is typically overlooked for the catalytic conversion of small alkanes,[40−42] it appears to play a more significant role in the dehydrogenative activation of more constrained PE substrate, by destabilizing the system by 15−27 kJ/mol for single-chain and crystalline PE, respectively (Figure 1). The β-hydride elimination step proceeds through a four-membered transition

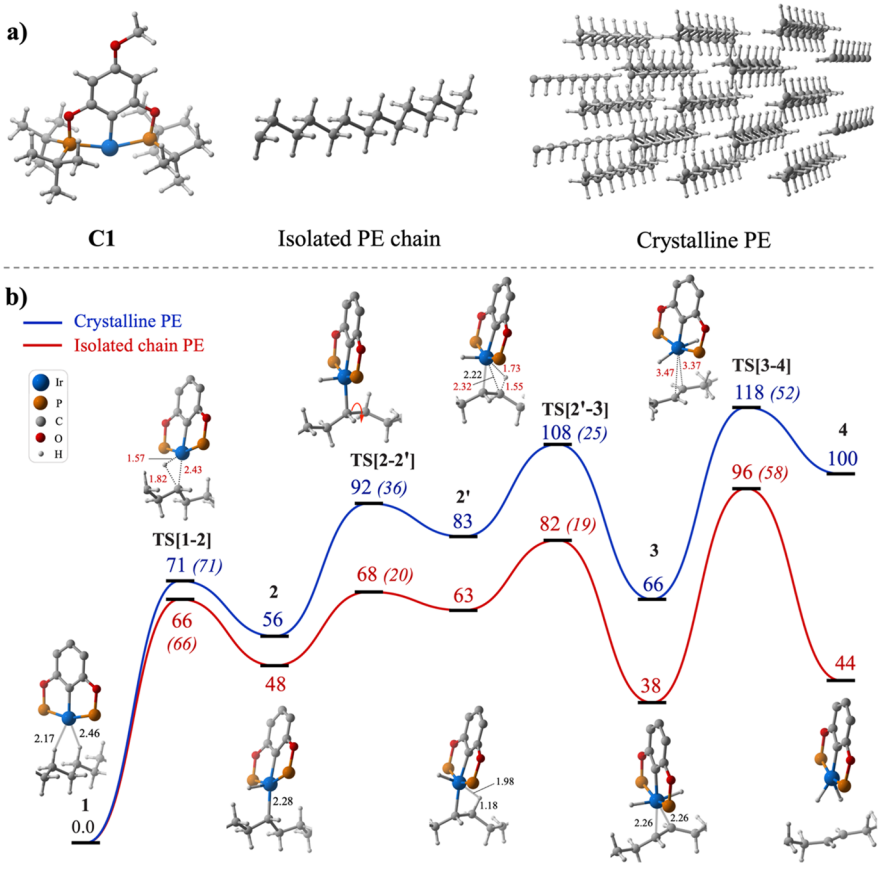

Figure 1. a) Optimized geometries of the model catalyst and pristine PE substrate. b) Computed reaction energy (kJ/mol) profile for the PE dehydrogenation by the (^{tBu4}POCOP)-Ir complex. The σ-complex of the active 14-electron (^{tBu4}POCOP)-Ir catalyst with PE was set as a reference. Intrinsic barriers for elementary steps with respect to the preceding intermediate are given in parentheses. OMe and H on the aryl and ^{t}Bu-fragments on P in the Ir catalyst have been omitted for clarity. Selected interatomic distances are in Å.

https://doi.org/10.1021/acscatal.3c03269
ACS Catal. 2023, 13, 13310−13318

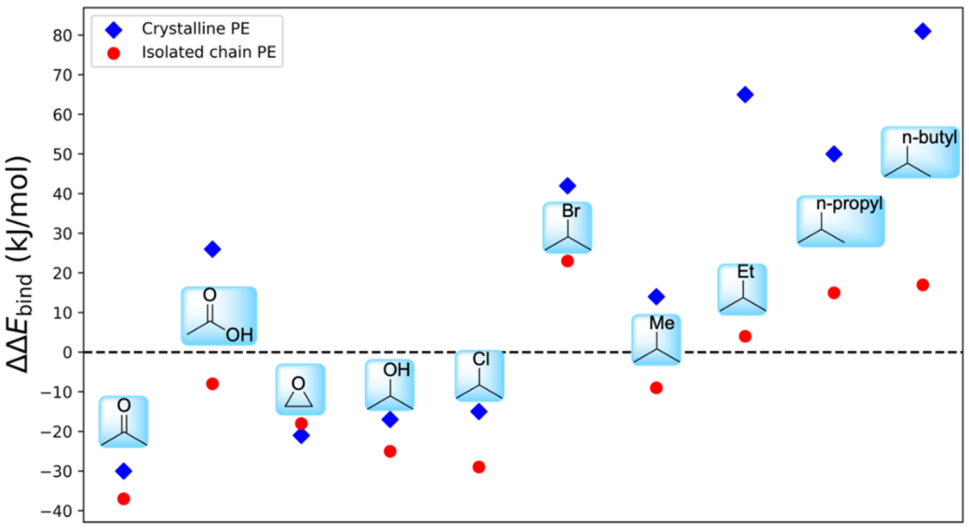

Figure 2. Relative catalyst-substrate binding energies ($\Delta\Delta E_{bind}$'s) for different functional groups with respect to the catalyst-pristine PE complex.

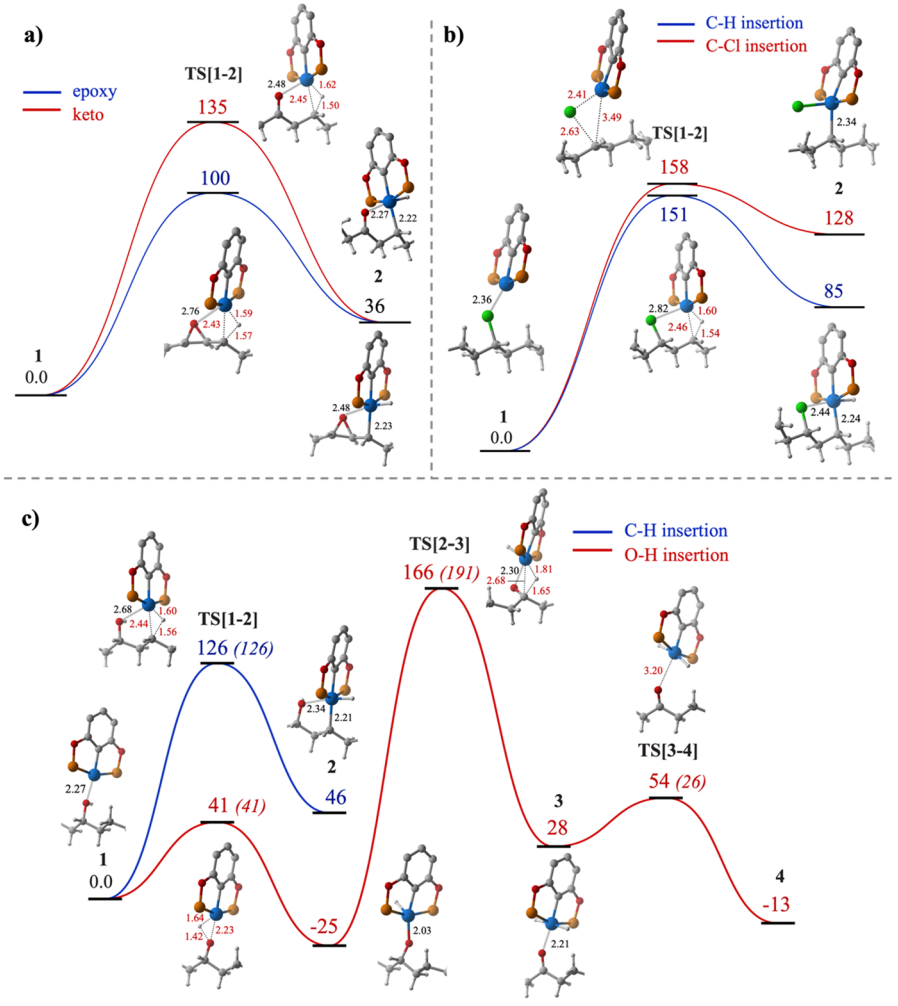

Figure 3. Computed reaction energy (kJ/mol) profile for (a) the C−H bond insertion on the keto- and epoxide-functionalized isolated PE chain models; (b) C−H and C−Cl bond insertions on the chlorine-functionalized isolated PE chain model; (c) possible dehydrogenation pathways of PE with a hydroxyl group. Intrinsic barriers for elementary steps with respect to the preceding intermediate are given in parentheses. OMe and H on the aryl and ^{t}Bu-fragments have been omitted for clarity. Selected optimized interatomic distances are in Å.

state [**TS(2′-3)**] with a barrier of 19 kJ/mol. Finally, the dehydrogenated PE chain dissociates [**TS(3−4)**] from the metal center and leaves (^{tBu4}POCOP)-IrH$_2$ species **4** which has a higher activation barrier of 58 kJ/mol. As all steps are reversible, an overall barrier is calculated with respect to the initial complex **1**.

https://doi.org/10.1021/acscatal.3c03269
ACS Catal. 2023, 13, 13310−13318

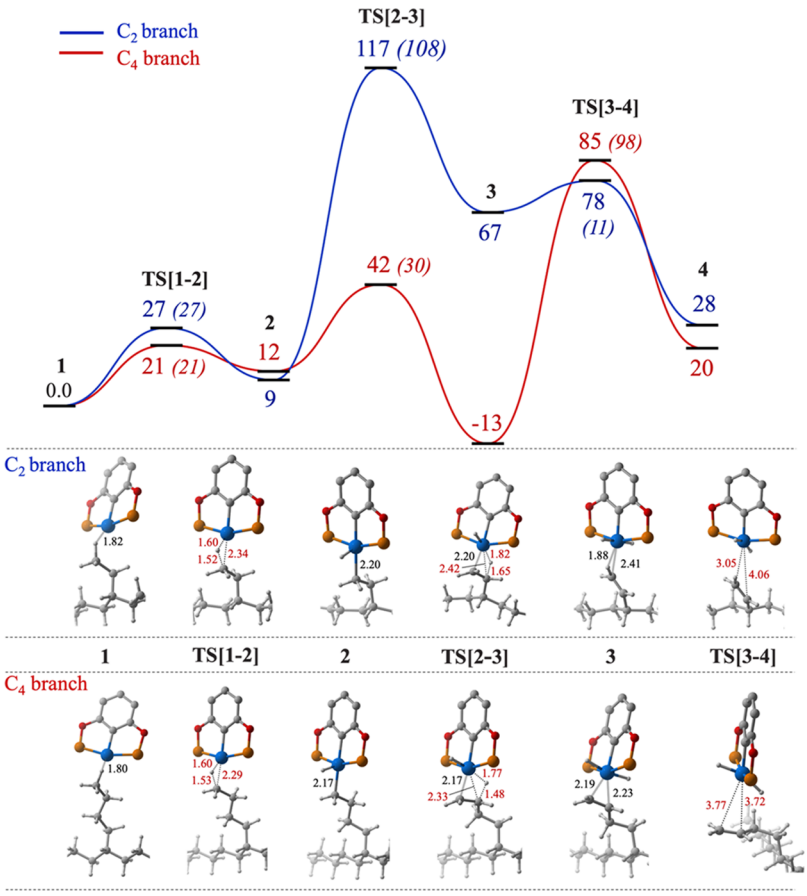

Figure 4. Computed reaction energy (kJ/mol) profiles for the dehydrogenation of the C_2- and C_4-branches on an isolated PE chain model. Intrinsic barriers for elementary steps with respect to the preceding intermediate are given in parentheses. OMe and H on the aryl and tBu-fragments are omitted for clarity, and selected interatomic distances are in Å.

The highest overall barrier, 96 kJ/mol, observed for alkene dissociation along the pathway is in line with the previous mechanistic study on homogeneous dehydrogenation of hexane.[40,42] The C−H oxidative addition energy barrier in crystalline PE is comparable to that in the isolated chain. The conformational change in the crystalline PE intermediate **3** distorts the crystalline packing resulting in a higher overall barrier (92 kJ/mol) compared to the isolated chain (68 kJ/mol). The preceding reaction steps also exhibit a higher energy barrier in the crystalline PE possibly due to distorted packing. Comparing the trends for the ideal crystalline PE surface and the isolated chain, we observed that the energy of the former steadily increases along the dehydrogenation path due to the steric effects of the bulky *tert*-butyl group and neighboring PE chain interaction. While the trend of intrinsic reactivity for both cases remains the same, the chain rotation and the distortion of packing shift the potential energy surface (PES) of crystalline PE dehydrogenation toward higher energies.

For the model of the crystalline PE, we assumed a perfect *all-trans* conformation. In practice, conformationally disordered chains could be found in PE,[19,43,44] which could significantly influence the reactivity. Indeed, the DFT calculations on a PE model representing the conformationally disordered PE chains (Figures S1−S2) reveal a much lower barrier for the initial C−H insertion step (37 vs 66 kJ/mol for the distorted and perfect PE models, respectively). On the other hand, the reaction of the PE chain with the gauche−trans−gauche conformation (Figure S1b) exhibits significantly higher β-hydride elimination and ligand loss barriers (Figure S2b). This emphasizes the importance of the in-chain mobility and conformation on the catalyst performance. Therefore, the steric effects of the interaction of the homogeneous dehydrogenation catalyst with the substrate and mobility of the substrate could drastically affect the intrinsic reactivity, suggesting that similar effects can be also observed in the presence of different PE imperfections.

3.2. Dehydrogenation of the PE with in-Chain Impurities. To assess the impact of the in-chain impurities on the PE dehydrogenation, we prepared different models featuring the keto group, epoxide, hydroxyl group, carboxyl group, chlorine, bromine, and C_nH_{2n+1} branches (n = 1−4).[19,21,45,46] We start with an analysis of the influence of such functional groups on the initial binding of the catalyst with the PE substrate. Figure 2 summarizes the DFT-computed binding energies ($\Delta\Delta E_{bind}$) with the values listed in Table S1.

Negative $\Delta\Delta E_{bind}$ values indicate a thermodynamic preference for the Ir pincer complex to interact with specific sites rather than with the virgin PE. Such a preference is observed for the carbonyl, epoxide, hydroxyl, and chlorine-functionalized PE models. Unexpectedly, no strong interactions were detected for the molecular complexes formed with the carboxyl and bromine functionalities in the PE.

The decreased thermodynamic preference in binding to longer branches and the carboxyl group at the surface of the crystalline PE can be attributed to the steric bulk of the pincer catalyst. Indeed, in the case of crystalline PE, the binding energy of the σ-complex is dominated by the dispersion interactions

https://doi.org/10.1021/acscatal.3c03269
ACS Catal. 2023, 13, 13310−13318

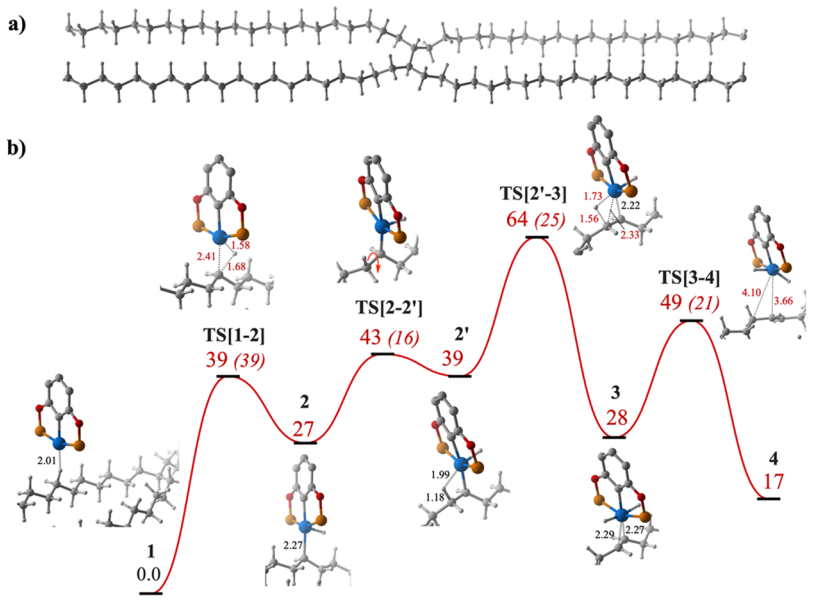

Figure 5. (a) Cross-linked polyethylene model and (b) computed reaction energy (kJ/mol) profile for cross-linked PE dehydrogenation. Intrinsic barriers for elementary steps with respect to the preceding intermediate are given in parentheses. OMe and H on the aryl and tBu-fragments were omitted for clarity. Selected interatomic distances are in Å.

between the bulky *tert*-butyl groups on the pincer arms and the neighboring chains. The interaction of the Ir pincer with the branches distant from the surface results in much fewer intermolecular contacts than with the extended surface and, accordingly, a lower overall binding energy.

While the high $\Delta\Delta E_{bind}$ indicates the preferential interactions of the catalyst with specific PE functional groups, it does not necessarily imply the deactivation of the catalyst molecule. These interactions could, on the contrary, promote the subsequent transformations or open alternative reaction paths.

Oxygen- and Chlorine-Functionalized PE. We next turned our attention to the impact of the PE imperfections with the lowest $\Delta\Delta E$ values (carbonyl, hydroxyl, epoxide, and chlorine) on the dehydrogenation reaction paths. Additionally, we examined the reactions occurring on two different alkyl branches (C_2 and C_4).

The C−H activation step with the carbonyl-adsorbed catalyst (Figure 3a) has a significantly higher (by ca. 70 kJ/mol) barrier compared to virgin PE. In addition, the progress of the reaction is obstructed since one of the coordination sites in the Ir sphere is occupied by the carbonyl oxygen (Ir−O distance equals 2.27 Å) in the resulting Ir(III) intermediate **2**. To proceed with the reaction, rotation along the C−Ir axis is necessary. However, this rotation is hindered by the bulky *tert*-butyl groups on the P donors, while complete dissociation of the complex from the surface C═O moiety would inquire substantial energy loss. Although the C−H activation of the epoxide-functionalized PE proceeds with a somewhat lower barrier of 100 kJ/mol, a similar deactivating effect is observed in this case. This suggests that oxo-functionalization of PE with carbonyl and epoxy-moieties would inhibit the dehydrogenation activity of the Ir pincer catalyst by preventing the formation of the initial σ-complex and hindering the reaction path.

Similarly, the presence of Cl on the PE chain hampers dehydrogenative activation with the Ir pincer (Figure 3b). Two alternative pathways were considered in this case, namely the C−H or C−Cl bond insertion paths. Both paths proceed with very high barriers of >150 kJ/mol due to the strong catalyst-substrate complex through the Ir−Cl interaction.

The reaction with the OH-modified PE may proceed via two alternative reaction paths, namely, starting with the oxidative addition of C−H or O−H bonds (Figure 3c). In the C−H bond insertion path, the Ir center coordinated to the hydroxyl oxygen oxidatively adds an adjacent C−H bond. Similar to the cases discussed above, this step proceeds with a very high barrier of 126 kJ/mol and yields an octahedral Ir surface complex, which hinders further progress of the catalytic cycle. An alternative alcohol dehydrogenation path proceeds via the catalyst O−H bond insertion resulting in an intermediate **3** with an Ir−O bond.[47] Although this path starts with a low barrier of only 40 kJ/mol, the subsequent β-H elimination step faces a prohibitively high barrier of 191 kJ/mol and yields the keto-functionalized PE chain.

Branched and Cross-Linked PE. The chemical polyolefin upcycling strategies proposed thus far emphasize the importance of the selective activation of the main chain of the polymer. The catalytic dehydrogenative activation of the polyolefin can potentially take place at both the main chain and the branches, thus affecting the overall process efficiency. To understand the differences in the respective catalytic paths, we next computed the reaction path for Ir-catalyzed dehydrogenation of the ethyl and *n*-butyl groups to model the reaction on the side branches (Figure 4).

The oxidative addition at the highly accessible terminal methyl group on the branches has a barrier of only 21−27 kJ/mol, which is much lower compared to that computed for the PE backbone. The size of the side chain has a pronounced effect on the next β-hydride elimination step. For the C_2H_5−PE model, a 3-fold higher barrier (108 kJ/mol) is computed than that for the *n*-Bu-modified PE because the bulky *tert*-butyl groups prevent stabilization of the π-complex of the catalyst with the vinyl group; instead, the σ-complex of [Ir−2H] with C−H of the vinyl group is formed. Indeed, the vinyl group is perpendicular to the PE backbone, and the Ir catalyst cannot properly coordinate to the double bond. Such an effect was not observed for the

https://doi.org/10.1021/acscatal.3c03269
ACS Catal. 2023, 13, 13310−13318

extended *n*-Bu side chain. Similar to the case for the pristine PE, in the *n*-Bu-PE model, the decomposition of the π-complex is the rate-limiting step. Thus, our calculations reveal the much more favorable activation of the side branches of the PE compared to the main chain, in line with the experimental observations.[48]

We also examined the dehydrogenation of cross-linked PE to understand the potential effects of cross-linking between chains. To model cross-linked PE, we extended the PE chain length to 42 atoms and connected neighboring chains in the center (Figure 5a).[49] The C−H oxidative addition on the cross-link carbons was found to be highly unfavorable. Therefore, we focused on studying the reaction occurring in eight carbons from the cross-links (Figure 5b). One notable observation is that the cross-linked chain exhibited slightly lower energy for the initial σ-complex formation compared to the non-cross-linked isolated chain PE (−80 kJ/mol vs −63 kJ/mol), despite the proximity between the chains, which prevents the bulky *t-Bu* ligand from embedding between them. The possible explanation for that is the dispersion interaction of the *tert*-butyl groups with the neighboring PE chain. The computed energy profile for the catalytic reaction shows similar trends to those for the isolated PE chain, although with barriers generally lower than the non-cross-linked PE, indicating a higher reactivity of such moieties and a potential promotion effect of PE cross-linking on the dehydrogenative upcycling with the homogeneous Ir catalyst.

The Impact of the Impurities. Our results show that the impurities in the polymer substrate have a profound influence on the catalyst performance. In this context, we formulated a simple numerical model to quantify the extent to which the catalyst becomes affixed to these impurities. For simplicity, we considered only oxygen and chlorine functional groups, assuming that all of the oxygen-containing impurities were present in the form of carbonyls. The top estimates for the practical concentration of impurities in postconsumption PE were obtained based on the work of Kusenberg et al.,[20] which reported oxygen and chlorine concentrations in the products of PE-film pyrolysis as 0.43 and 0.02 wt %, respectively. This can be considered a strongly contaminated postconsumption PE substrate, with the impurity concentrations of roughly 274 μmol impurities (268 μmol of carbonyl and 6 μmol of chlorine groups) per 1 g polymer. The successful experimental demonstration of the dehydrogenative PE upcycling with the Ir-(^{tBu}POCOP)-HCl molecular catalyst employed ca. 150 μmol of catalyst per 1 g of PE substrate.[17,18] This implies that when used with waste polyethylene as the substrate, the molecular catalyst, originally designed for synthetic chemistry applications, would likely experience strong inhibition due to the preferential competitive binding with the impurities within the PE chain. Therefore, further efforts toward more efficient catalytic plastic upcycling technologies should target minimization of the negative impact of the impurities. The polymer substrate can be pretreated prior to the catalytic upgrading to reduce the amount of heteroatoms via, for example, catalytic hydrotreatment.[20,50] One could also envisage the use of protecting groups or additives to mask the presence of strongly coordinating functional groups in the polymer, but this approach would lead to additional complications of the overall process. The more targeted catalyst design strategy also presents an attractive route, in which one aims at a catalyst that concurrently manifests enhanced activity and robustness against impurities. An ideal catalyst should show a limited affinity to functional groups, while being still highly reactive and selective toward inert C−H groups.

4. CONCLUSIONS

In this computational study, we investigated the reaction pathways of PE dehydrogenation with different functional groups using a model homogeneous (^{tBu4}POCOP)-Ir catalyst. Our findings indicate that the catalyst performance could be significantly inhibited in the presence of in-chain impurities such as carbonyl, hydroxyl, epoxides, and chlorine functionalities. These impurities hinder the reaction by forming stable molecular complexes with the catalyst, increasing the barrier for the initial C−H bond activation step and saturating the coordination sphere of the Ir catalyst.

Structural imperfections of the PE structure, such as the presence of branches or cross-links, also have a profound impact on the performance of the Ir catalyst. Smaller branches on the PE chain can be reversibly activated by the Ir catalyst, although their dehydrogenation is kinetically limited by a high barrier for the β-H elimination step. Longer and more flexible branches can serve as the preferential sites for the catalytic activation, thus reducing the overall efficiency of the upcycling depolymerization process. The presence of cross-links in the PE structure also facilitates the dehydrogenative conversion path with the bulky Ir pincer catalyst.

Overall, our study highlights the importance of considering the presence of in-chain impurities for the chemical recycling of plastics. It emphasizes the need to use model catalysts with specific functional groups or to conduct studies on fresh and aged polyethylene chains to better understand the impact of impurities or aging on the reaction process. These insights contribute to a broader understanding of catalyst deactivation mechanisms and can guide the development of more efficient catalysts and processes for PE recycling and valorization.

■ ASSOCIATED CONTENT

Data Availability Statement

Data related to this publication is available *via* the 4TU database under the DOI 10.4121/26af8ffb-1aeb-4d33-8005-b7d888c5a8f5.

Supporting Information

The Supporting Information is available free of charge at https://pubs.acs.org/doi/10.1021/acscatal.3c03269.

Binding energy values and the reaction paths on distorted PE chains (PDF)

Optimized structures in the VASP POSCAR format (ZIP)

■ AUTHOR INFORMATION

Corresponding Author

Evgeny A. Pidko − *Inorganic Systems Engineering, Department of Chemical Engineering, Faculty of Applied Sciences, Delft University of Technology, Delft 2629 HZ, Netherlands;* orcid.org/0000-0001-9242-9901; Email: e.a.pidko@tudelft.nl

Authors

Alexander A. Kolganov − *Inorganic Systems Engineering, Department of Chemical Engineering, Faculty of Applied Sciences, Delft University of Technology, Delft 2629 HZ, Netherlands;* orcid.org/0000-0002-0262-8892

A. Sreenithya − *Inorganic Systems Engineering, Department of Chemical Engineering, Faculty of Applied Sciences, Delft University of Technology, Delft 2629 HZ, Netherlands*

Complete contact information is available at: https://pubs.acs.org/10.1021/acscatal.3c03269

Author Contributions

The manuscript was written through contributions of all authors. All authors have given approval to the final version of the manuscript.

Notes

The authors declare no competing financial interest.

■ ACKNOWLEDGMENTS

The authors acknowledge the use of computational resources of DelftBlue supercomputer, provided by Delft High Performance Computing Centre (https://www.tudelft.nl/dhpc). The authors thank Advanced Research Center Chemical Building Blocks Consortium (ARC CBBC) for supporting this research under project number 2021.038.C.

■ REFERENCES

(1) Geyer, R.; Jambeck, J. R.; Law, K. L. Production, use, and fate of all plastics ever made. *Science Advances* **2017**, *3* (7), No. e1700782.

(2) Garcia, J. M.; Robertson, M. L. The future of plastics recycling. *Science* **2017**, *358* (6365), 870−872.

(3) Billiet, S.; Trenor, S. R. 100th Anniversary of Macromolecular Science Viewpoint: Needs for Plastics Packaging Circularity. *ACS Macro Lett.* **2020**, *9* (9), 1376−1390.

(4) Chu, M.; Liu, Y.; Lou, X.; Zhang, Q.; Chen, J. Rational Design of Chemical Catalysis for Plastic Recycling. *ACS Catal.* **2022**, *12* (8), 4659−4679.

(5) Vollmer, I.; Jenks, M. J. F.; Roelands, M. C. P.; White, R. J.; van Harmelen, T.; de Wild, P.; van der Laan, G. P.; Meirer, F.; Keurentjes, J. T. F.; Weckhuysen, B. M. Beyond Mechanical Recycling: Giving New Life to Plastic Waste. *Angew. Chem., Int. Ed.* **2020**, *59* (36), 15402−15423.

(6) Akubo, K.; Nahil, M. A.; Williams, P. T. Aromatic fuel oils produced from the pyrolysis-catalysis of polyethylene plastic with metal-impregnated zeolite catalysts. *Journal of the Energy Institute* **2019**, *92* (1), 195−202.

(7) Kunwar, B.; Moser, B. R.; Chandrasekaran, S. R.; Rajagopalan, N.; Sharma, B. K. Catalytic and thermal depolymerization of low value post-consumer high density polyethylene plastic. *Energy* **2016**, *111*, 884−892.

(8) Yu, H.; Li, F.; He, W.; Song, C.; Zhang, Y.; Li, Z.; Lin, H. Synthesis of micro−mesoporous ZSM-5 zeolite with microcrystalline cellulose as co-template and catalytic cracking of polyolefin plastics. *RSC Adv.* **2020**, *10* (37), 22126−22136.

(9) Aguado, J.; Sotelo, J. L.; Serrano, D. P.; Calles, J. A.; Escola, J. M. Catalytic Conversion of Polyolefins into Liquid Fuels over MCM-41: Comparison with ZSM-5 and Amorphous SiO2−Al2O3. *Energy Fuels* **1997**, *11* (6), 1225−1231.

(10) Sánchez-Rivera, K. L.; Huber, G. W. Catalytic Hydrogenolysis of Polyolefins into Alkanes. *ACS Central Science* **2021**, *7* (1), 17−19.

(11) Celik, G.; Kennedy, R. M.; Hackler, R. A.; Ferrandon, M.; Tennakoon, A.; Patnaik, S.; LaPointe, A. M.; Ammal, S. C.; Heyden, A.; Perras, F. A.; et al. Upcycling Single-Use Polyethylene into High-Quality Liquid Products. *ACS Central Science* **2019**, *5* (11), 1795−1803.

(12) Onwudili, J. A.; Williams, P. T. Catalytic supercritical water gasification of plastics with supported RuO2: A potential solution to hydrocarbons−water pollution problem. *Process Safety and Environmental Protection* **2016**, *102*, 140−149.

(13) Yao, L.; King, J.; Wu, D.; Chuang, S. S. C.; Peng, Z. Non-thermal plasma-assisted hydrogenolysis of polyethylene to light hydrocarbons. *Catal. Commun.* **2021**, *150*, No. 106274.

(14) Kim, S.; Sin, A.; Nam, H.; Park, Y.; Lee, H.; Han, C. Advanced oxidation processes for microplastics degradation: A recent trend. *Chemical Engineering Journal Advances* **2022**, *9*, No. 100213.

(15) Amelia, D.; Fathul Karamah, E.; Mahardika, M.; Syafri, E.; Mavinkere Rangappa, S.; Siengchin, S.; Asrofi, M. Effect of advanced oxidation process for chemical structure changes of polyethylene microplastics. *Materials Today: Proceedings* **2022**, *52*, 2501−2504.

(16) Wang, N. M.; Strong, G.; DaSilva, V.; Gao, L.; Huacuja, R.; Konstantinov, I. A.; Rosen, M. S.; Nett, A. J.; Ewart, S.; Geyer, R.; et al. Chemical Recycling of Polyethylene by Tandem Catalytic Conversion to Propylene. *J. Am. Chem. Soc.* **2022**, *144* (40), 18526−18531.

(17) Arroyave, A.; Cui, S.; Lopez, J. C.; Kocen, A. L.; LaPointe, A. M.; Delferro, M.; Coates, G. W. Catalytic Chemical Recycling of Post-Consumer Polyethylene. *J. Am. Chem. Soc.* **2022**, *144* (51), 23280−23285.

(18) Conk, R. J.; Hanna, S.; Shi, J. X.; Yang, J.; Ciccia, N. R.; Qi, L.; Bloomer, B. J.; Heuvel, S.; Wills, T.; Su, J.; et al. Catalytic deconstruction of waste polyethylene with ethylene to form propylene. *Science* **2022**, *377* (6614), 1561−1566.

(19) Chen, L.; Huan, T. D.; Ramprasad, R. Electronic Structure of Polyethylene: Role of Chemical, Morphological and Interfacial Complexity. *Sci. Rep.* **2017**, *7* (1), 6128.

(20) Kusenberg, M.; Roosen, M.; Zayoud, A.; Djokic, M. R.; Dao Thi, H.; De Meester, S.; Ragaert, K.; Kresovic, U.; Van Geem, K. M. Assessing the feasibility of chemical recycling via steam cracking of untreated plastic waste pyrolysis oils: Feedstock impurities, product yields and coke formation. *Waste Management* **2022**, *141*, 104−114.

(21) Chen, Q.; Wang, Q.; Zhang, C.; Zhang, J.; Dong, Z.; Xu, Q. Aging simulation of thin-film plastics in different environments to examine the formation of microplastic. *Water Res.* **2021**, *202*, No. 117462.

(22) Gijsman, P.; Meijers, G.; Vitarelli, G. Comparison of the UV-degradation chemistry of polypropylene, polyethylene, polyamide 6 and polybutylene terephthalate. *Polym. Degrad. Stab.* **1999**, *65* (3), 433−441.

(23) Gulmine, J. V.; Janissek, P. R.; Heise, H. M.; Akcelrud, L. Degradation profile of polyethylene after artificial accelerated weathering. *Polym. Degrad. Stab.* **2003**, *79* (3), 385−397.

(24) Ragaert, K.; Delva, L.; Van Geem, K. Mechanical and chemical recycling of solid plastic waste. *Waste Management* **2017**, *69*, 24−58.

(25) Du, J.; Zeng, L.; Yan, T.; Wang, C.; Wang, M.; Luo, L.; Wu, W.; Peng, Z.; Li, H.; Zeng, J. Efficient solvent- and hydrogen-free upcycling of high-density polyethylene into separable cyclic hydrocarbons. *Nat. Nanotechnol.* **2023**, *18*, 772.

(26) Wang, Y.; Hu, P.; Yang, J.; Zhu, Y.-A.; Chen, D. C−H bond activation in light alkanes: a theoretical perspective. *Chem. Soc. Rev.* **2021**, *50* (7), 4299−4358.

(27) Abdelgaid, M.; Mpourmpakis, G. Structure−Activity Relationships in Lewis Acid−Base Heterogeneous Catalysis. *ACS Catal.* **2022**, *12* (8), 4268−4289.

(28) Chen, X.; Peng, M.; Xiao, D.; Liu, H.; Ma, D. Fully Exposed Metal Clusters: Fabrication and Application in Alkane Dehydrogenation. *ACS Catal.* **2022**, *12* (20), 12720−12743.

(29) Mavrantza, I.-E.; Prentzas, D.; Mavrantzas, V. G.; Galiotis, C. Detailed atomistic molecular-dynamics simulation of the orthorhombic phase of crystalline polyethylene and alkane crystals. *J. Chem. Phys.* **2001**, *115* (8), 3937−3950.

(30) Galimberti, D.; Milani, A.; Maschio, L.; Castiglioni, C. Intermolecular modulation of IR intensities in the solid state. The role of weak interactions in polyethylene crystal: A computational DFT study. *J. Chem. Phys.* **2016**, *145* (14), 144901.

(31) Kresse, G.; Joubert, D. From ultrasoft pseudopotentials to the projector augmented-wave method. *Phys. Rev. B* **1999**, *59* (3), 1758−1775.

(32) Kresse, G.; Furthmüller, J. Efficient iterative schemes for ab initio total-energy calculations using a plane-wave basis set. *Phys. Rev. B* **1996**, *54* (16), 11169−11186.

(33) Perdew, J. P.; Burke, K.; Ernzerhof, M. Generalized Gradient Approximation Made Simple. *Phys. Rev. Lett.* **1996**, *77* (18), 3865−3868.
(34) Goerigk, L.; Grimme, S. Accurate Dispersion-Corrected Density Functionals for General Chemistry Applications. In *Modeling of Molecular Properties*; 2011; pp 1−16.
(35) Grimme, S.; Ehrlich, S.; Goerigk, L. Effect of the damping function in dispersion corrected density functional theory. *J. Comput. Chem.* **2011**, *32* (7), 1456−1465.
(36) Mathew, K.; Kolluru, V. S. C.; Mula, S.; Steinmann, S. N.; Hennig, R. G. Implicit self-consistent electrolyte model in plane-wave density-functional theory. *J. Chem. Phys.* **2019**, *151* (23), 234101.
(37) Mathew, K.; Sundararaman, R.; Letchworth-Weaver, K.; Arias, T. A.; Hennig, R. G. Implicit solvation model for density-functional study of nanocrystal surfaces and reaction pathways. *J. Chem. Phys.* **2014**, *140* (8), No. 084106.
(38) Blöchl, P. E. Projector augmented-wave method. *Phys. Rev. B* **1994**, *50* (24), 17953−17979.
(39) Henkelman, G.; Uberuaga, B. P.; Jónsson, H. A climbing image nudged elastic band method for finding saddle points and minimum energy paths. *J. Chem. Phys.* **2000**, *113* (22), 9901−9904.
(40) Biswas, S.; Blessent, M. J.; Gordon, B. M.; Zhou, T.; Malakar, S.; Wang, D. Y.; Krogh-Jespersen, K.; Goldman, A. S. Origin of Regioselectivity in the Dehydrogenation of Alkanes by Pincer−Iridium Complexes: A Combined Experimental and Computational Study. *ACS Catal.* **2021**, *11* (19), 12038−12051.
(41) Kumar, A.; Zhou, T.; Emge, T. J.; Mironov, O.; Saxton, R. J.; Krogh-Jespersen, K.; Goldman, A. S. Dehydrogenation of n-Alkanes by Solid-Phase Molecular Pincer-Iridium Catalysts. High Yields of α-Olefin Product. *J. Am. Chem. Soc.* **2015**, *137* (31), 9894−9911.
(42) Gordon, B. M.; Lease, N.; Emge, T. J.; Hasanayn, F.; Goldman, A. S. Reactivity of Iridium Complexes of a Triphosphorus-Pincer Ligand Based on a Secondary Phosphine. Catalytic Alkane Dehydrogenation and the Origin of Extremely High Activity. *J. Am. Chem. Soc.* **2022**, *144* (9), 4133−4146.
(43) Snyder, R. G.; Poore, M. W. Conformational Structure of Polyethylene Chains from the Infrared Spectrum of the Partially Deuterated Polymer. *Macromolecules* **1973**, *6* (5), 708−715.
(44) Urban, M. W. Fourier Transform Infrared and Fourier Transform Raman Spectroscopy of Polymers. In *Structure-Property Relations in Polymers, Advances in Chemistry*; American Chemical Society: 1993; Vol. *236*, pp 3−40.
(45) Corrales, T.; Catalina, F.; Peinado, C.; Allen, N. S.; Fontan, E. Photooxidative and thermal degradation of polyethylenes: interrelationship by chemiluminescence, thermal gravimetric analysis and FTIR data. *J. Photochem. Photobiol., A* **2002**, *147* (3), 213−224.
(46) Tarducci, C.; Kinmond, E. J.; Badyal, J. P. S.; Brewer, S. A.; Willis, C. Epoxide-Functionalized Solid Surfaces. *Chem. Mater.* **2000**, *12* (7), 1884−1889.
(47) Polukeev, A. V.; Abdelaziz, O. Y.; Wendt, O. F. Combined Experimental and Computational Study of the Mechanism of Acceptorless Alcohol Dehydrogenation by POCOP Iridium Pincer Complexes. *Organometallics* **2022**, *41* (7), 859−873.
(48) Ray, A.; Zhu, K.; Kissin, Y. V.; Cherian, A. E.; Coates, G. W.; Goldman, A. S. Dehydrogenation of aliphatic polyolefins catalyzed by pincer-ligated iridium complexes. *Chem. Commun.* **2005**, *27*, 3388−3390.
(49) Blaško, M.; Mach, P.; Antušek, A.; Urban, M. DFT Modeling of Cross-Linked Polyethylene: Role of Gold Atoms and Dispersion Interactions. *J. Phys. Chem. A* **2018**, *122* (5), 1496−1503.
(50) Liu, S.; Kots, P. A.; Vance, B. C.; Danielson, A.; Vlachos, D. G. Plastic waste to fuels by hydrocracking at mild conditions. *Science Advances* **2021**, *7* (17), No. eabf8283.

https://doi.org/10.1021/acscatal.3c03269
ACS Catal. 2023, 13, 13310−13318